A THESIS FOR THE DEGREE OF MASTER OF SCIENCE

Analyses of Light Interception and Photosynthetic Rate of Sweet Pepper (*Capsicum annuum*) Plants Based on Structural Accuracy of 3D Plant Model

3 차원 식물 모델의 구조적 정확도에 따른 파프리카의 수광 및 광합성 분석

BY

DONGPIL KIM

FEBRUARY, 2019

MAJOR IN HORTICULTURAL SCIENCE AND BIOTECHNOLOGY
DEPARTMENT OF PLANT SCIENCE
GRADUATE SCHOOL
COLLEGE OF AGRICULTURE AND LIFE SCIENCES
SEOUL NATIONAL UNIVERSITY

Analyses of Light Interception and Photosynthetic Rate of Sweet Pepper (*Capsicum annuum*) Plants Based on Structural Accuracy of 3D Plant Model

UNDER THE DIRECTION OF DR. JUNG EEK SON SUBMITTED TO THE FACULTY OF THE GRADUATE SCHOOL OF SEOUL NATIONAL UNIVERSITY

BY

DONGPIL KIM

DEPARTMENT OF PLANT SCIENCE

SEOUL NATIONAL UNIVERSITY

FEBRUARY, 2019

APPROVED AS A QUALIFIED THESIS OF DONGPIL KIM FOR THE DEGREE OF MASTER OF SCIENCE BY THE COMMITTEE MEMBERS

CHAIRMAN _____

HEE JAE LEE, Ph.D.

VICE-CHAIRMAN _____

JUNG EEK SON, Ph.D.

MEMBER _____

CHANGHOO CHUN, Ph.D.

Analyses of Light Interception and Photosynthetic Rate of Sweet Pepper (*Capsicum annuum*) plants Based on Structural Accuracy of 3D Plant Model

Dongpil Kim

Department of Plant Science, Graduate School of Seoul National University

ABSTRACT

Plant structure is one of the determinant factors of light environment and subsequent photosynthesis productivity. Traditional functional-structural plant model (FSPM) has been used for exploring plant light environment, but the model could affect the result of light interception and subsequent photosynthesis due to issue on structural fidelity. The aim of this study is to investigate the difference between light interception and photosynthesis results in a model reconstructed through a 3D scanner and conventional static FSPM. At single-leaf and whole plant levels, a model reconstructed directly from scanned data was compared with a static FSPM created indirectly by substituting the measured structural variables in commercial plant modeling software. Ray-tracing was performed on both models with the same simulation condition, and photosynthesis was calculated by using Farquhar-von Caemmerer-Berry (FvCB) model with results of light interception at leaf and plant levels. As a result, the light interception was overestimated by traditional

static FSPM because of omission of fine structure such as vein, and the subsequent photosynthesis was also highly evaluated by the difference of light intensity distribution according to the structural expression. In whole plant scale, confirmed to be light interception and photosynthetic rate were 30 and 59% higher, respectively. Therefore, light interception and photosynthesis could be more precisely analyzed by using the 3D-scanned plant model.

Additional key words: light interception, paprika, photosynthesis, plant model, plant structure, ray-tracing

Student number: 2017-23974

CONTENTS

LIST OF TABLES

LIST OF FIGURES

INTRODUCTION

Light interception by the plant canopy is a crucial factor in plant development and biomass accumulation associated with photosynthesis (Purcell et al., 2002), as well as photomorphogenesis (Ballaré et al., 1995). The geometrical structure of a plant is highly correlated with its light-harvesting efficiency (Niinemets, 2007).

However, it is difficult to analyze the light distribution in a canopy due to the high spatial complexity of canopy components (Baldocchi and Collineau, 1994). To overcome such complexities, in-silico ray-tracing (Cieslak et al., 2008) and radiosity (Chelle and Andrieu, 1998) methods have been applied to virtual plants to analyze light interception in more detail. The geometrical accuracy of the plant model can have a significant effect on inferences about light interception and subsequent photosynthesis rates calculated based on light simulation (Salikioti et al., 2011). However, the sophistication of existing plant models varies depending on the purpose of the simulation or the type of crop being simulated.

Existing functional-structural plant models (FSPMs), when combined with process-based models, can be used to represent plant spatial geometry at various levels of detail ranging from accurate descriptions of each organ (e.g., leaf, stem) to coarse descriptions of branching systems at the plant level (Godin and Sinoquet, 2005). FSPM studies have assessed the effect of architectural

variation on light interception by implementing ray-tracing simulations on structural models with scales from the phytomer level (e.g., leaf angle, ratio of leaf length and width) to developmental stages (Falster and Westoby, 2003; Sarlikioti et al., 2011a; Barillot et al., 2014) because FSPMs of each modular plant organ can be assembled.

Rule-based FSPMs have been optimized for testing and visualization based on dynamic processes of the plant, but structural descriptions of these rule-based FSPMs tend to be unsophisticated because simple plant growth models and measurement references are used (De Reffye et al., 2009). In contrast, a static FSPM can describe plants at specific growth stages based on direct measurement of the plant at the organ level and can depict more detail than rule-based plant models (Vos et al., 2010). However, static FSPMs do not provide a detailed description of structure at the phytomer level (e.g., leaf vein) and have a different appearance from the actual plant.

Several studies have extracted structure directly from the plant being studied and used these models to analyze the light environment of the plant (Retkute et al., 2018; Townsend et al., 2018). Direct modeling methods extract the plant structure directly using a 3D scanner and the structure-from-motion imaging technique to construct a 3D plant mesh, enabling a more realistic representation of the plant (Lou et al., 2014; Paulus et al., 2014; Moriondo et al., 2016; Zhang et al., 2016). The reconstructed model can be visualized in 3D space through software tools (e.g., computer-aided design; CAD), and the light environment

of the plant canopy can be analyzed using the ray-tracing method, which simulates trajectories of numerous light rays (De Visser et al., 2014).

Direct modeling methods can be used to analyze the effect of light interception by plant structures with more realistic features by combining a phenotypic model with simulations using a structural model (Burgess et al., 2015). Compared to FSPM, there is no procedure for manual measurement, and a 3D reconstruction method can easily be used. However, a bottleneck associated with the direct modeling method is reconstruction of the entire plant structure at high resolution. In particular, the structures of greenhouse-grown crops are more difficult to obtain by 3D scanning because the crops are densely packed and are maintained to have a high leaf area index to improve productivity (Van der Heijden et al., 2012).

The aim of this study was to develop a parametric model of greenhouse-grown sweet pepper plants based on 3D-scanned data and a direct modelling method, verify the structural accuracy of the model, and analyze if there were differences in light interception and photosynthesis rates between structurally accurate models and other existing models.

LITERATURE REVIEW

3D plant model

Structural modeling of 3D plant is the first step for analyzing plant light environment through *in-silico* method. The initial form of plant model called L-system, a modular approach that combines computer language with plant topology and branching morphogenesis (Lindenmayer, 1968; Prusinkiewicz and Hanan., 1990). Subsequently, the static FSPM enabled a more elaborate description of the plant by depicting the plant model with substituting geometrical variables of the plant such as leaf width, leaf angle, tiller number, or stem length based on the L-system (Vos et al., 2010).

Limitation of previous plant modeling method

FSPM studies clearly access the effect of architectural variation on light interception by implementing ray-tracing simulation on structural model with scale varies on phytomer level, developmental stages, and different genotypes (Falster and Westoby, 2003; Sarlikioti et al., 2011a; Barillot et al., 2014; Burgess et al., 2017). However, FSPM has an issue on their structural expression because the plant model depicted on a regular basis, ranging from simple descriptions with branching rule to varies on accurate descriptions on phytomer units. Thus, the light interception and photosynthesis could be

changed according to the structural expression when the model is used for ray-tracing simulation.

Ray-tracing simulation methods

For ray-tracing simulation, a nested radiosity method (Chelle and Andrieu, 1998) and Quais-Monte Carlo method with FSPM (Cieslak et al., 2008) has been used. Recently, a reverse ray-tracing method was also used to reduce errors from plant structure (Bailey, 2018).

3D reconstruction of plant model

Recently, several studies have been conducted to extract structure of the plant directly with 3D scanner or stereovision method (Barth et al., 2018; Townsend et al., 2018). These studies suggest that the methods of direct modeling of plant structure show high reliability in the structure.

MATERIALS AND METHODS

Workflow

Figure 1 shows the workflow from reconstructing the plant structural model to light interception and photosynthesis analyses. In the direct method, the plant model was reconstructed directly from 3D scanned data, while in the indirect method, the plant model was constructed by inputting structural parameters into plant modelling software (Fig. 2). Because the same plants were used for the experiments, the overall shapes were similar. The 3D scanned mesh included fine details of the leaf structure such as veins, while leaves reconstructed using the indirect model had a simpler surface. Light interception was analyzed using the ray-tracing method for the directly and indirectly reconstructed models under the same simulation conditions, and photosynthesis was evaluated by applying a photosynthesis model to the ray-tracing results. Finally, differences in light interception and photosynthesis for the two plant models were evaluated.

Model definitions and fidelity

Direct plant models were reconstructed using mesh data obtained from 3D scanning, and then the mesh data were analyzed using parametric models compatible with CAD software. For use with 3D CAD software, the mesh data have to be converted to a parametric surface through a reverse design process. Transformed model named as a scanned parametric model (PM), The directly

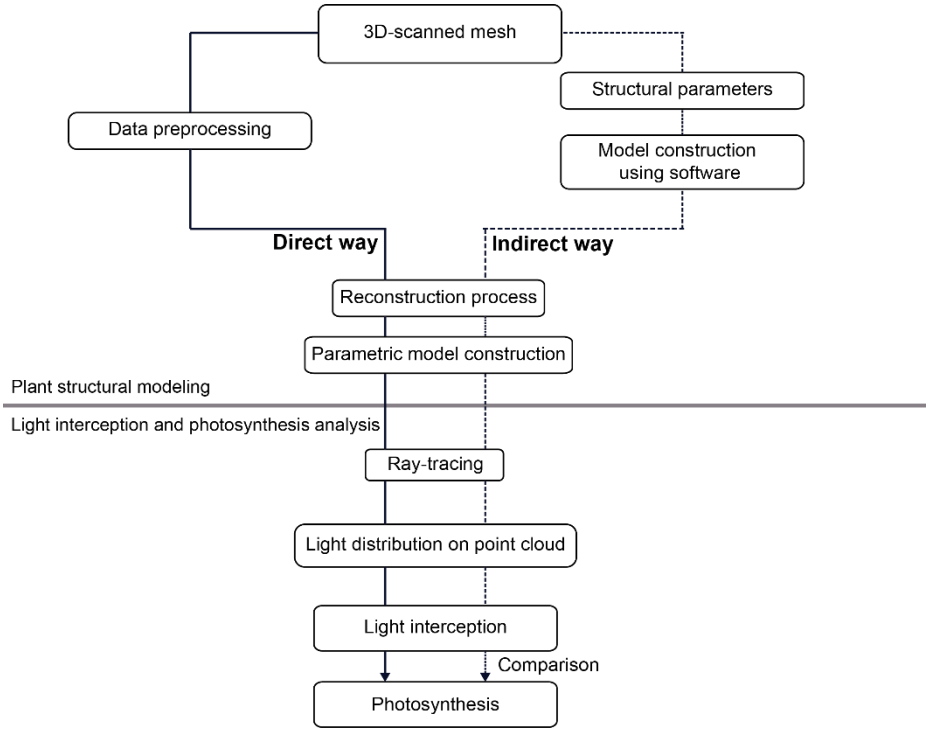

Fig. 1. Workflow from plant 3D scanning to photosynthesis analysis.

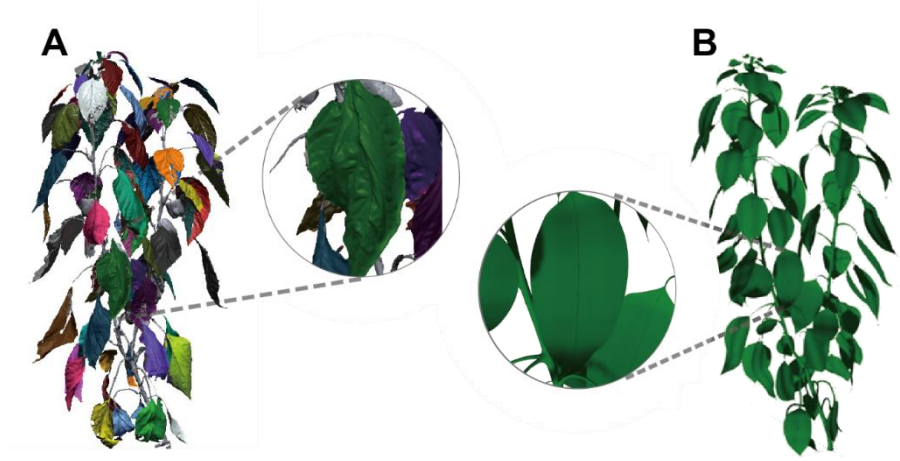

Fig. 2. View of a reconstructed mesh obtained by 3D scan (A) and a mesh created by commercial software (B). Enlarged view shows leaf precision for each model.

reconstructed model was defined as scanned PM at leaf and whole-plant levels. Indirectly reconstructed model like the static FSPM model; these comprised a low-curvature PM at the leaf level and an indirectly reconstructed PM at the whole-plant level. The fidelity of the created PM to the scan mesh was evaluated based on geometrical tolerance. Geometric tolerances were analyzed using the Accuracy Analyzer™ function of Geomagic Design X, which is a reverse engineering software (3D Systems, Rockhill, SC, USA).

Plant material

Sweet pepper (*Capsicum annuum* L., cv. Scirocco) plants were cultivated on rock-wool slab with a planting density of 2 plants m^{-2} in a Venlo-type glasshouse at the Protected Horticulture Research Institute, National Institute of Horticultural and Herbal Sciences, Rural Development Administration, Haman, Korea (N35.2°, E128.4°). Sweet pepper plants were seeded on May 31, 2017, and transplanted on July 7, 2017. During the seedling period, electrical conductivity (EC) of the nutrient solutions was 0.8 dS m^{-1} and was gradually increased by 0.2 dS m^{-1} and maintained at 2.5 dS m^{-1} until transplant. After transplanting, 33 mL of a nutrient solution of EC 2.5 dS m^{-1} and pH 6.0 was supplied 14 times a day per plant by drip irrigation. Plants were pruned to two main stems, which were vertically trellised to a 'V' canopy system (Jovicich et al., 2004).

3D scan of plant structure

3D scans of sweet pepper plants was obtained at 75 days after transplanting, on September 19, 2017, using a high-resolution portable 3D scanner (GO!SCAN50TM, CREAFORM, Lévis, Quebec, Canada) and scan software (Vxelement 6.0, CREAFORM). We obtained point cloud data comprising x, y, and z positions and R, G, B color information for each point. After scanning a sweet pepper plant, scanned mesh data were segmented into individual leaves, stems, and fruits (Fig. 2A), while imperfections such as holes and floating fragments were corrected with reverse engineering software (Geomagic Design X, 3D Systems). After preprocessing of the mesh data, leaf area of the scanned mesh was extracted. Scanned mesh was converted to a PM to perform optical simulations with the same software (Fig. 3B). Leaf area was measured using a leaf area meter (LI-3100, LI-COR, Lincoln, NE, USA) to compare the actual leaf area with the leaf area derived from the scanned mesh.

Indirect reconstruction of plant model

To compare 3D-scanned PMs to indirectly reconstructed PMs, models were indirectly reconstructed at leaf and whole-plant levels. At the leaf level, a low-curvature leaf PM was created based on the scanned model by omitting structural details based on leaf outlines (Fig. 4B). At the whole-plant level, a plant structure model was constructed by inputting structural parameters into Plant Factory 2016 R6 Studio software (EON Software, Paris, France).

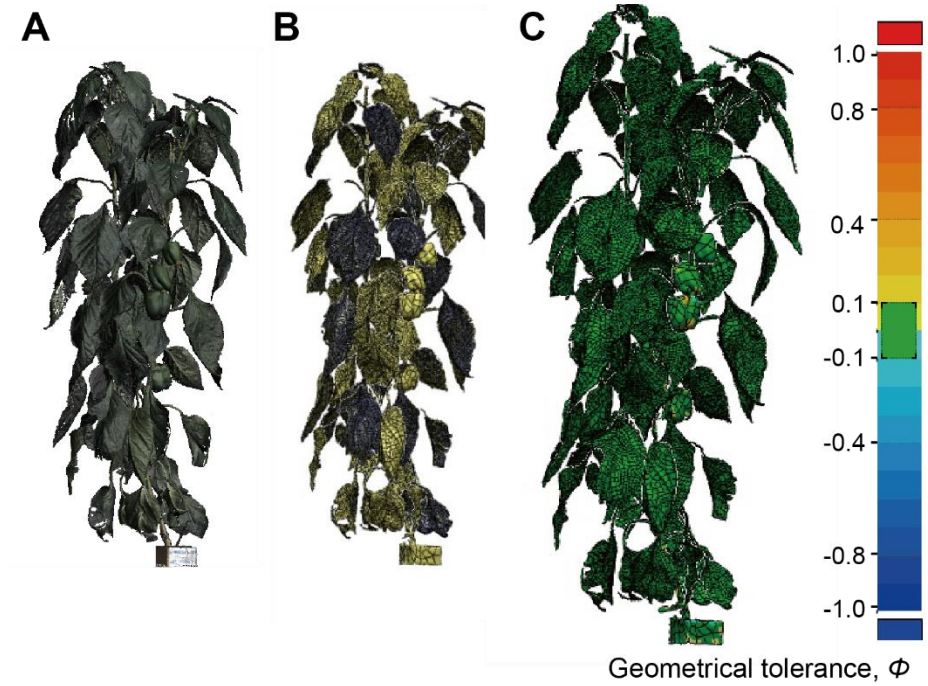

Fig. 3. Parametric reconstruction process and fidelity analysis of sweet pepper plants. (A) Original 3D-scanned mesh of sweet pepper, (B) reconstructed parametric model, and (C) geometric tolerance of the mesh and parametric models.

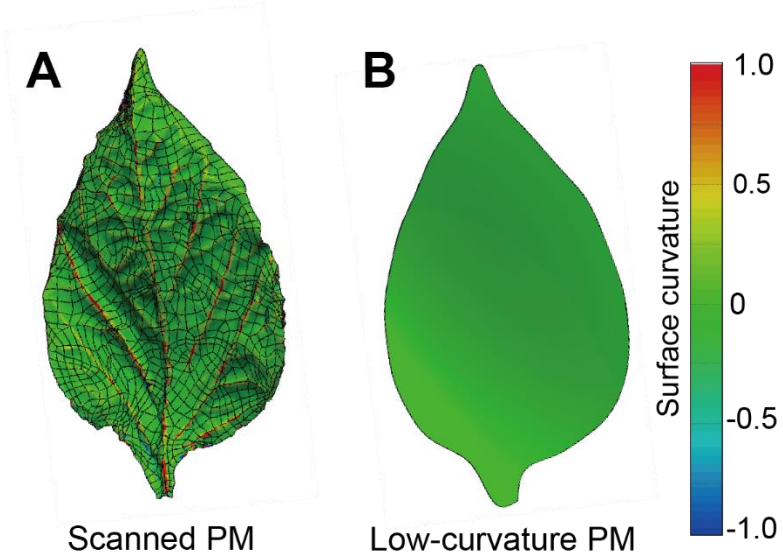

Fig. 4. Leaf surface curvature for leaves of different precision estimated by the scanned parametric model (A) and low-curvature parametric model (B).

Parameters used for reconstruction were leaf length, leaf width, petiole length, internode length, leaf distribution, and leaf angle, the latter which is defined as the angle of the normal vector of the leaf plane with respect to the zenith (Hosoi and Omasa, 2015).

Leaf optical properties

Light transmittance and reflectance of sweet pepper leaves were measured in the range of 300 to 900 nm with a spectroradiometer (BLUE-Wave Spectrometer, StellarNet Inc., Tampa, FL, USA), a solar simulator (XIL-01B50KPV1, SERIC Ltd., Tokyo, Japan), and an integrating sphere (IC-2, StellarNet Inc.). Leaves were sampled individually at the bottom, middle, and top of the sweet pepper canopy. Because there were no significant difference in optical properties among these canopy positions, mean values of the three positions were used in the ray-tracing simulations (Fig. S1). Measured leaf optical properties were used for simulation in the photosynthetically active radiation range of 400-700 nm.

Simulation environment and conditions

Constructed 3D plant models were transferred to 3D CAD software (SOLIDWORKS, Dassault Systemes, Vélizy-Villacoublay, France), and light interception was simulated using ray-tracing software (OPTISWORKS, OPTIS Inc., La Farlède, France). Light interception was simulated on the 3D-scanned

PMs and indirectly reconstructed PMs under the same conditions. In the leaf-level simulation, a direct light source was modeled, and the angle between the light source and leaf was set to −90 to 90° at 30° intervals to compare the pattern of light interception according to leaf structure and incoming radiation angle (Fig. S2A). In the whole-plant simulation, the ambient lighting source feature in Optiswork was used to simulate natural global light with direct and scattered light. Simulation parameters were set to equatorial (N0°, E0°) and equinox (March 21, 2018), 12:00. The solar azimuth at this time was 89° 44 '26.434". The turbidity value was set to 3, which represents a general clear day. For these conditions, the ratio of direct to scattered light was about 6:4. In CAD software, plants were arranged in 3x3 isotropic form, and the row distance of individual plants was set to 40 cm (Fig. S2B). For accurate ray-tracing simulation, the total number of rays was set to 1 giga-ray in all experiments.

Calculation of photosynthesis rate

Leaf photosynthesis rate was calculated by the modified Farquhar, von Caemmerer, and Berry (FvCB) model of Qian et al. (2012). Photosynthetic parameters (V_{max}, J_{max}) were calculated from non-linear regression analysis of leaf photosynthesis measurements at the top, middle, and bottom of the canopy using a portable photosynthesis system (LI-COR) (Table S1). V_{max} and J_{max} were assumed to decay exponentially with canopy depth, and these three positions were interpolated by regression. R_{ac} and R_{aj} were assumed to have a

constant value of 0.11, and α and θ parameters were fixed at 0.8 and 0.15, respectively, as described by Kim et al. (2016). Temperature and relative humidity were fixed at 25˚C and 65%, respectively. To use the model to estimate the single variable function of light intensity, leaf CO_2 concentration was fixed to 400 ppm. The single variable function of light intensity was expressed as

$$A = \sum_{i=0}^{n} \min\{A_C(i)\ , A_j(i)\} \qquad \text{Equation 1}$$

where i is light intensity at each point cloud, A (µmol m^{-2} s^{-1}) is net photosynthesis rate, A_c (µmol m^{-2} s^{-1}) is ribulose 1,5-bisphosphate carboxylase/oxygenase carboxylation-limited photosynthesis rate, and A_j (µmol m^{-2} s^{-1}) is ribulose 1,5-biphosphate regeneration-limited photosynthesis rate. For the leaf-scale experiment, photosynthetic parameters from the top layer were used to estimate photosynthesis.

RESULTS

Validation of structural reconstruction

In the leaf-scanned PM, surface curvatures were wider and higher than in the low-curvature PM (Fig. 4). In particular, surface curvature was larger along the leaf vein but did not change along the leaf vein in the simplified shape of the slow-curvature PM. The R^2 value was 0.98 between leaf area extracted from the scanned mesh and leaf area measured with a leaf area meter. The mean absolute percentage error was 7.89, similar to the value of the existing measurement method (Fig. S3). Scanned PM area was not significantly different than that of the scan mesh. Leaf areas of six samples in the low-curvature PM were significantly lower by 14 to 38% than those in the original mesh ($P < 0.001$) (Table 1). Leaf area was reduced by 38% in leaf sample 4 and was different between the model and reality when the leaf had a more wrapped-up and complex structure. At the whole-plant level, the geometric tolerance between the scanned mesh and reconstructed scanned PM was less than 0.1 mm in most areas except for complex structures such as fruit (Fig. 3C).

Light interception pattern at the leaf scale

At the leaf level, the light interception pattern varied according to incoming radiation angle (Fig. 5B). In the scanned PM, less light was intercepted along the curvature of the leaf; in the low-curvature PM, leaves uniformly intercepted

Table 1. Leaf area estimated by scanned mesh data, scanned parametric model, and low-curvature parametric model. The individual ratios of (B) or (C) to (A) were averages of six leaves.

Model	Leaf area (cm^2)						
	1	2	3	4	5	6	Ratio
Scanned mesh (A)	363.9	355.3	341.5	237.2	189.1	182.7	1.00 a[z]
Scanned PM (B)	360.7	352.8	352.8	236.0	179.6	188.8	1.01 a
Low-curvature PM (C)	313.6	310.1	277.7	171.2	147.6	138.3	0.81 b

[z]Different letters within a column indicate statistically significant differences by ANOVA at $P < 0.001$.

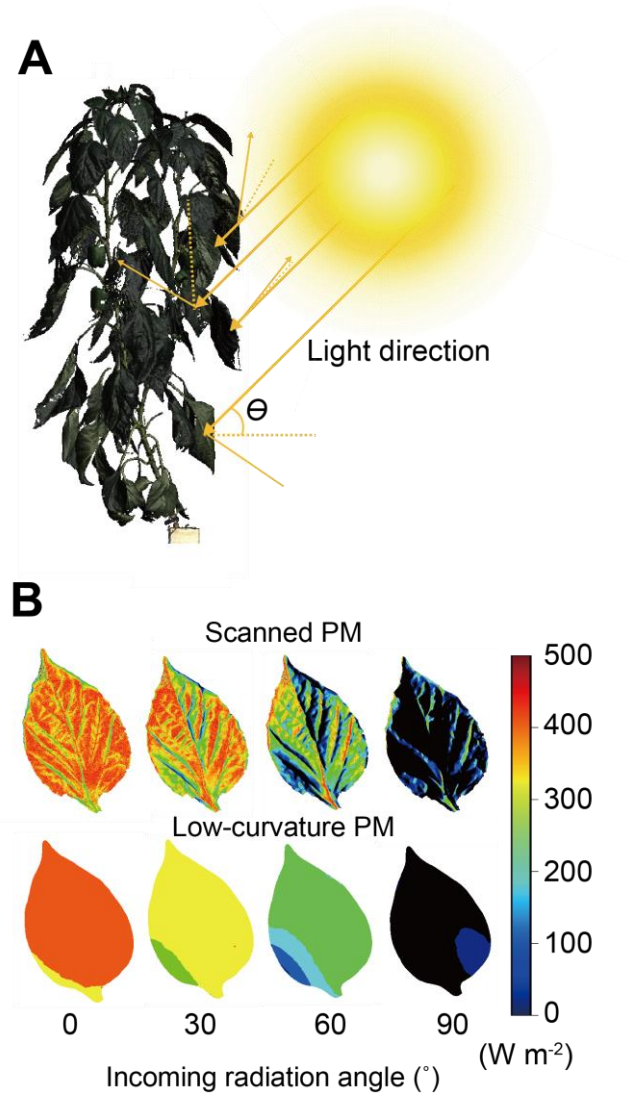

Fig. 5. Light interception of leaves according to light direction. (A) Schematic view of light direction to leaves, (B) light distributions on leaves of the scanned parametric model (top) and the low-curvature parametric model (bottom).

light. Light interception was higher with a smaller incoming radiation angle and varied by leaf depending on radiation angle and leaf shape (Fig. 6). When the incoming radiation angle was 0°, the mean light interception was 306.2 ± 31.73 W m^{-2} (mean ± SD; n = 6) for the scanned PM and 378.2 ± 18.44 W m^{-2} (n = 6) for the low-curvature PM. Light interception was about 1.23 times higher for the low-curvature PM than the scanned PM (Fig. 7A). When the incoming radiation angle was 90° or −90°, 109.8 ± 63.09 W m^{-2} (n = 12) light was intercepted by the low-curvature PM and 63.4 ± 51.08 W m^{-2} (mean ± SD; n = 12) light by the scanned PM. In leaf sample 2, there was variation in light intensity of the two models, as shown by the histogram in Fig. 7B. The scanned PMs covered a broad range of light intensities from low to high, with a high frequency of low light intensity (0-50 µmol m^{-2} s^{-1}). In the low-curvature PM, most light intensities were clustered near the mean value. The ratio of the light intercepted by the low-curvature PM versus the scanned PM was 1.2:1 for a 0° incoming radiation angle, but the ratio decreased to less than 1.0 as the incoming radiation angle increased (Fig. 8A). In leaf sample 2, standard deviations of light interception values were 111.4 and 9.3 W m^{-2} for the scanned PM and low-curvature PM, respectively. Standard deviations were higher for the scanned PM than the low-curvature PM regardless of the incoming radiation angle (Fig. 8B).

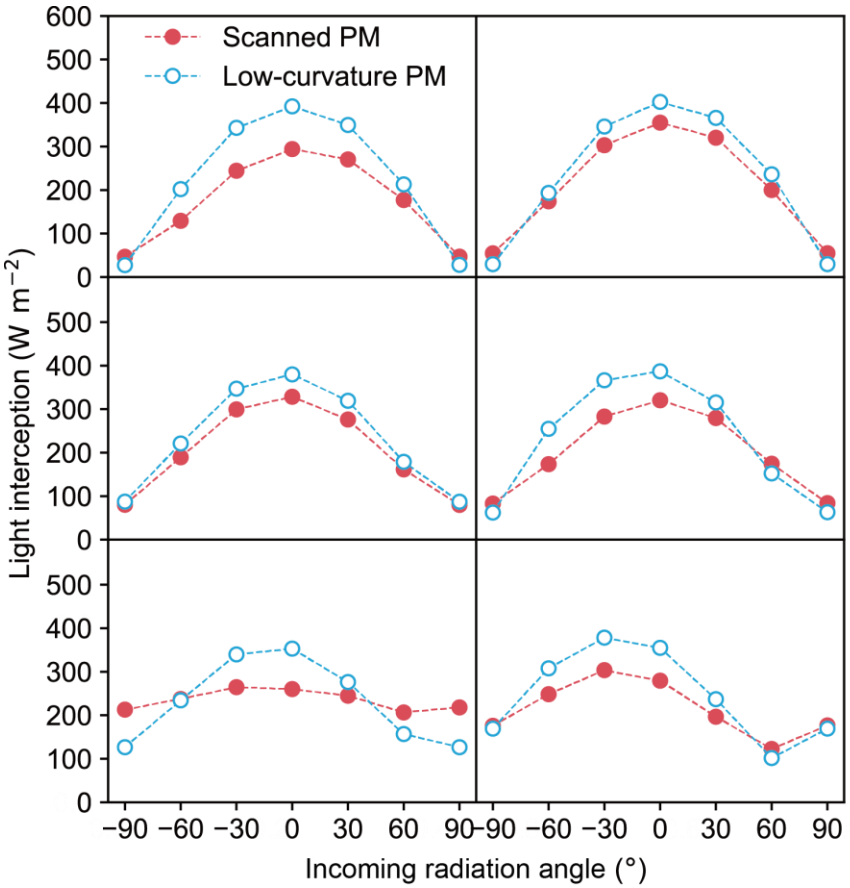

Fig. 6. Light interceptions of six sampled leaves according to light direction. Radiation at incoming angles of −90, −60, −30, 0, 30, 60, and 90° was applied to the leaf models. Sample number was the same as in Table 1 and Fig. S5.

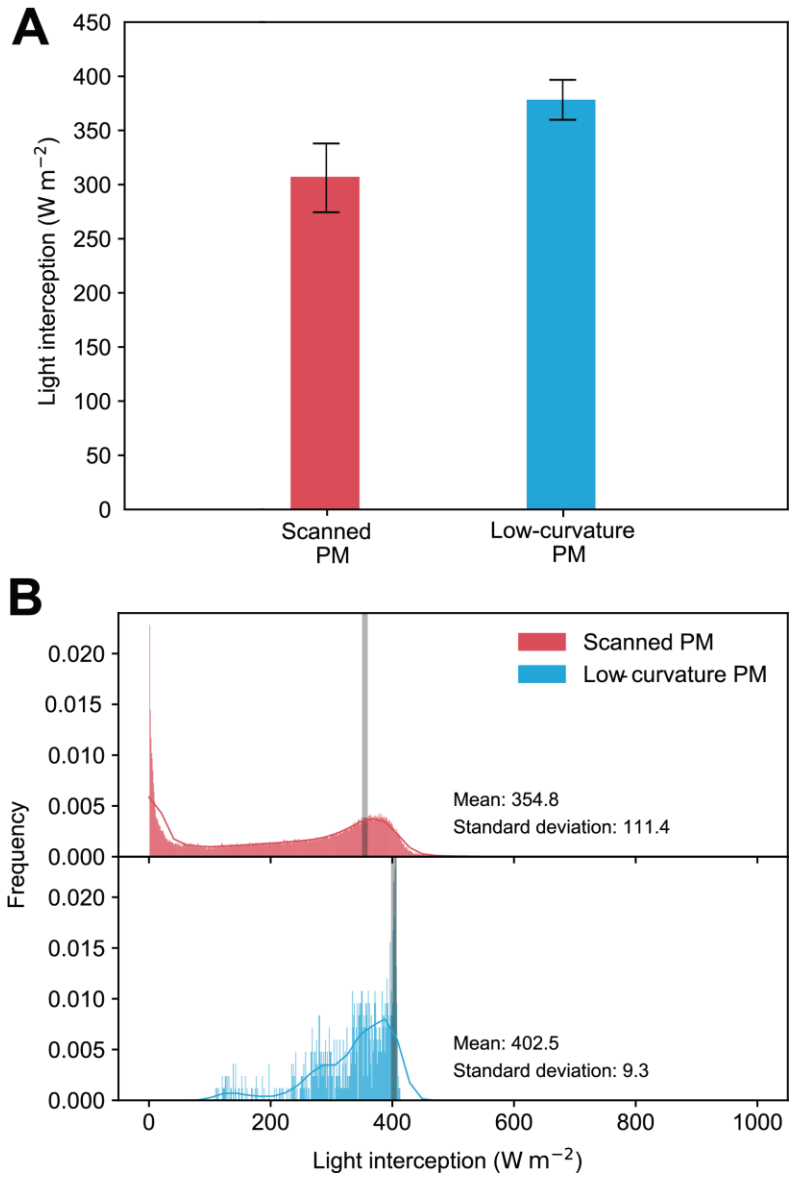

Fig. 7. Light interception and light distribution in different leaf models for an incoming radiation angle of 0º. (A) Light interceptions of two different structural models. Vertical bars represent mean ± SD (n = 6) of six leaves; (B) histograms of light distributions on the leaves.

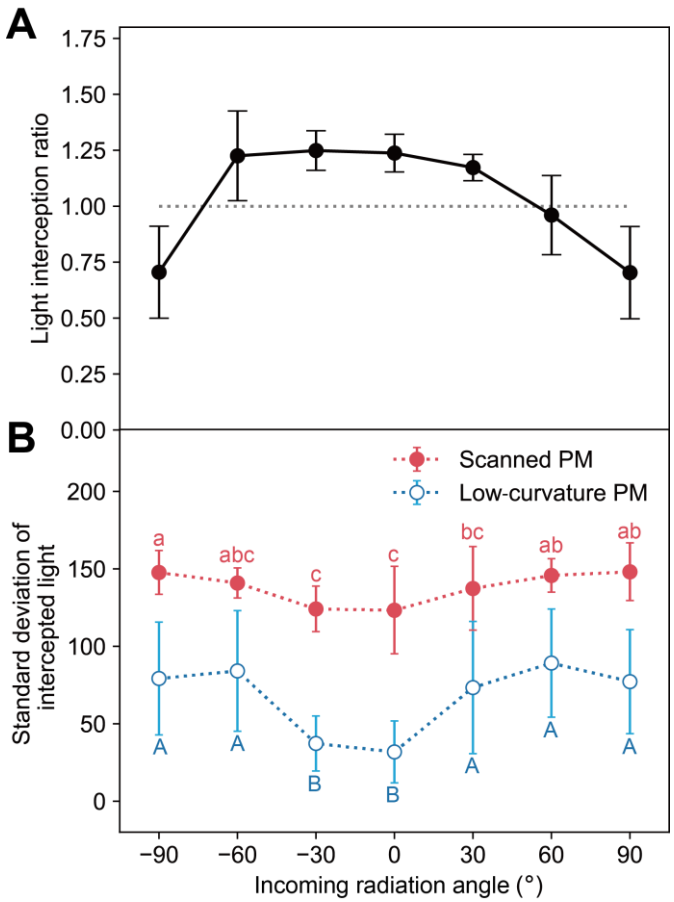

Fig. 8. Light interception amount and standard deviation according to incoming radiation angle estimated by the scanned parametric model and low-curvature model. (A) Light interception ratio of the low-curvature parametric model to that of the scanned parametric model; (B) standard deviation of light interception of the two different leaf models. Vertical bars indicate mean ± SD of six leaves. Same letters within models are not significantly different according to incoming radiation angle (Tukey HSD, $\alpha = 0.05$).

Estimated photosynthesis at the leaf and whole-plant levels

Photosynthesis in leaves was analyzed at incoming radiation angles of 0° and 90°. Photosynthetic rates for the low-curvature PM were higher than those for the scanned PM at all light intensities (Fig. 9). Photosynthesis was calculated by summing the photosynthetic rate values corresponding to the respective light intensities in the leaf and whole-plant (Fig. 9A). Photosynthesis rate was lower at an incoming radiation angle of 90° than at an angle of 0° in both models (Fig. 9B). At the whole-plant level, mean light interception was 1.3 times higher in the indirectly reconstructed PM than in the scanned PM (Table 2). Mean photosynthetic rates of scanned and indirectly reconstructed PMs were 2.17 μmol m^{-2} s^{-1} and 3.49 μmol m^{-2} s^{-1}, respectively.

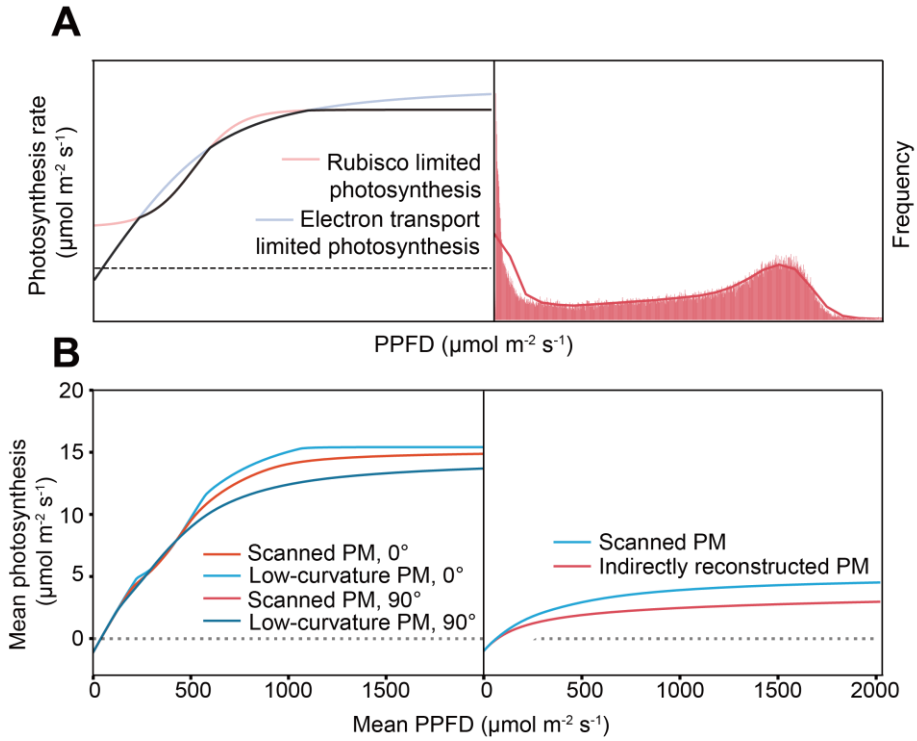

Fig. 9. Photosynthesis calculation based on intercepted light intensity and distribution of light intensities at the leaf and whole-plant levels. (A) Photosynthesis was calculated by summing photosynthetic rate values corresponding to the light intensities of each point cloud in the light-photosynthesis curve. Light-photosynthesis curve of the figure was drawn based on the FvCB model used in this experiment at leaf level. (B) Mean photosynthesis curve at the leaf level (leaf sample 2) and whole-plant level according to mean PPFD (0-2000 μmol m^{-2} s^{-1}).

Table 2**.** Mean values of light interception and photosynthetic rate at the whole-plant level estimated for the scanned PM and indirectly reconstructed PM.

Model	Light interception ($\mu mol\ m^{-2}\ s^{-1}$)	Mean photosynthetic rate ($\mu mol\ m^{-2}\ s^{-1}$)
Scanned PM (A)	583	2.17
Indirectly reconstructed PM (B)	758	3.49
B / A	1.30	1.59

DISCUSSION

Structural differences in plants inevitably result in differences in light interception. Canopy light interception varies depending on structural features of the plant such as leaf length-width ratio, leaf elevation angle, petiole length, leaf curvature, and phyllotatic angle (Niinemets and Fleck, 2002, Zotz et al., 2002, Sarlikioti et al., 2011a). Changes in light interception can clearly be explained by use of the plant structure as a variable at the overall canopy level. Light interception can change depending on the fidelity of the structural model used in optical simulation. In this study, it was demonstrated that the shape and quantity of light interception varied with fidelity of the plant model when the same structural parameters were used for plant reconstruction at the leaf and whole-plant levels.

The amount of light intercepted by the low-curvature PM was higher than that intercepted by the scanned PM, where the structure of the leaf was precisely expressed (Fig. 5B). Self-shading was observed along the vein in the scanned PM, and the amount of light intercepted by such an area was relatively lower than that in the low-curvature PM.

In an actual plant canopy, leaves are distributed at various angles and positions to intercept omnidirectional light (Fig. 5A). Therefore, light interception patterns of the two models were analyzed according to incoming radiation angle. Light interception was higher for the low-curvature PM for

radiation at an incoming angle of 0°, while that for the scanned PM was higher for radiation at an incoming angle of 90°, i.e., when all light was received from the side (Fig. 8). This variation in light interception could be due to the fact that highly curved leaves have larger areas for intercepting light from the side. This phenomenon is the same as reduction in light interception from the side when leaves are flat (Jordan and Smith, 1993).

Amount of light intercepted from the side was less than that intercepted from the front (Fig. 6). This is why the standard deviations of light interception between samples were higher at incoming radiation angles of 60° and 90° than at 0° and 30°. This tendency means that the amount of light received from the side is more affected by the structure of the leaf than the light received from the front. In this study, differences in light interception were analyzed according to fineness of the leaf structure and not differences in shape and curvature of a particular leaf. Researchers have attempted to geometrically define various leaf forms (Coussement et al., 2018; Zhang et al., 2017), but it remains challenging to define differences in light interception according to dynamic leaf morphology such as curviness and twistedness.

As the intensity and amount of light were changed, the photosynthesis rate changed in a curvilinear manner (Yin and Struik, 2009). Plants can use scattered light more efficiently than direct light (Farquhar and Roderick, 2003; Mercado et al., 2009). In fact, photosynthesis and crop production were confirmed to be enhanced with uniform light distribution from the canopy, which was achieved

by using scattered glass in the greenhouse (Li et al., 2016). Thus, photosynthetic efficiency changes according to the overall light intensity distribution in a plant. For the FvCB photosynthesis model, photosynthetic rates were determined by the position of the light curve corresponding to light intensity (Fig. 9A).

In the two models, the mean photosynthesis rate varied according to light intensity and distribution. In the leaf unit, the photosynthesis rates were higher in the low-curvature PM than in the scanned PM. This is because most of the light was located near the mean value in the low-curvature PM (Fig. 7B), indicating high photosynthetic efficiency. At the whole-plant level, the mean photosynthetic rate was also higher in the indirectly reconstructed PM than in the scanned PM (Table 2). The overall photosynthetic curve at the whole-plant level was located lower than the leaf level because the lower part of the canopy intercepted low light intensity due to mutual shading from plants (Fig. 10). V_{cmax} and J_{max}, indicators of leaf photosynthesis efficiency, were also lower at the bottom canopy, so the overall photosynthetic rate at the whole-plant level was lower than that at the leaf level, which was based on parameters measured at the top of the canopy. Photosynthesis efficiency was lower toward the bottom canopy and similar to that reported previously for sweet pepper (Kim et al., 2016).

In summary, light interception was 1.3 times higher in the indirectly reconstructed PM than in the scanned PM, and the mean photosynthesis rate was 1.59 times larger in the indirectly reconstructed PM than the scanned PM.

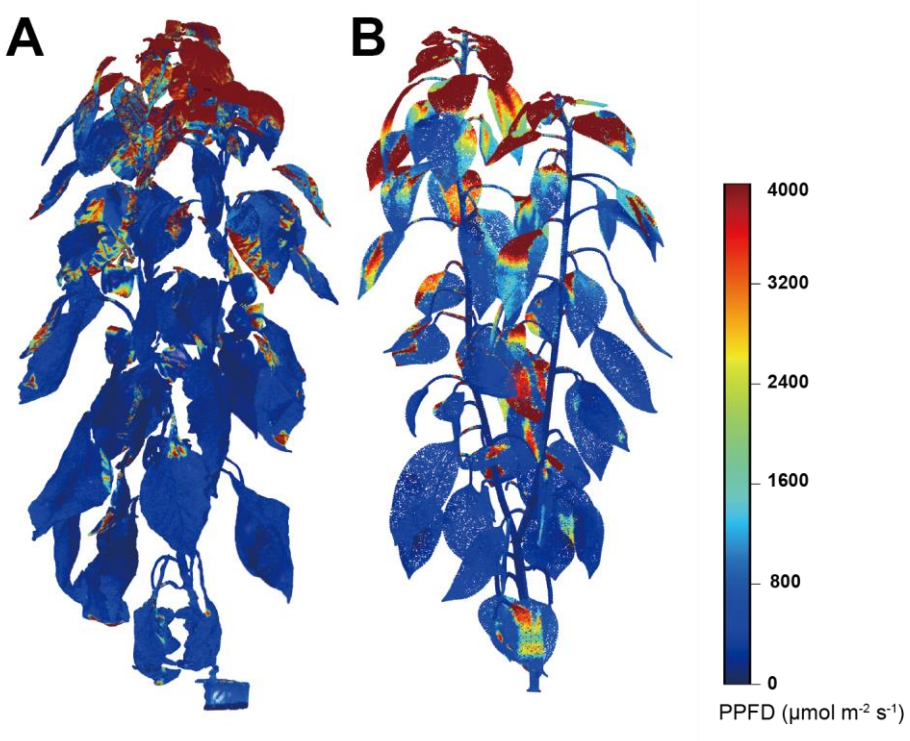

Fig. 10. Spatial light distributions within a whole-plant 3 x 3 isotropic arrangement. (A) Scanned parametric model, (B) low-curvature parametric model.

That means that photosynthesis differs depending on light distribution and intensity. Therefore, light interception and photosynthesis results could be biased when simulated using a simple plant model reconstructed through plant structural parameters (Sarlikioti et al., 2011b).

Scanned PMs can be used to accurately explicate photosynthesis for a wide range of light distribution. Thus, it is possible to quantitatively analyze photophysiology when there are dynamic fluctuations of leaf light environment using scanned PMs, whereas this was only previously possible by field experiment (Li et al., 2014). In addition, the geometry measurement process necessary for conventional indirect methods (Sinoquet et al., 1998), which is labor-intensive, can be omitted when using scanned PMs.

Three-dimensional monitoring techniques have facilitated acquisition of plant phenotype data and automatic measurement of plant parameters (Ubbens and Stavness, 2017; Chaudhury and Barron, 2018). In addition, direct plant models that can be hierarchically explained from geometrical parameters based on mesh data have been formulated (Barth et al., 2018; Wen et al., 2018). Thus, the future direction of plant structure modeling is likely to be a combination of direct modeling and parametrized structures to obtain versatile and realistic models. This will allow analysis of the influence of the light environment on the plant from various perspectives.

CONCLUSIONS

Light interception and photosynthesis may differ depending on structural precision of the plant model. Therefore, light interception and photosynthesis analysis were performed using two different plant models reconstructed by 3D scanning and traditional indirect method. The plant parametric model reconstructed from 3D scanned data had elaborate leaf details such as leaf veins and a twisted morphology, while the indirectly reconstructed model had a leaf shape that was more representative than detailed. Mean light interception amount and subsequent photosynthesis rates were 1.3-fold and 1.59-fold higher for the indirectly reconstructed plant model than the scanned PM, respectively. Light interception and photosynthesis results were observed to vary depending on amount of detail in the leaf model. Together, this results suggest that light interception can be more accurately investigated using a 3D scanned model than a conventional plant model. Scanned PM methodology can also be used for more accurate research into plant light environment or photosynthesis and photo-physiology.

LITERATURE CITED

Bailey BN (2018) A reverse ray-tracing method for modelling the net radiative flux in leaf-resolving plant canopy simulations. Ecol Model 368:233-245.

Baldocchi D, Collineau S (1994) The physical nature of solar radiation in heterogeneous canopies: Spatial and temporal attributes. Exploitation of Environmental Heterogeneity by Plants Ecophysiological Processes Above- and Belowground, 21-71.

Ballaré CL, Scopel AL, Sánchez RA (1995) Plant photomorphogenesis in canopies, crop growth, and yield. HortScience 30:1172-1181.

Barillot R, Escobar-Gutiérrez AJ, Fournier C, Huynh P, Combes D (2014) Assessing the effects of architectural variations on light partitioning within virtual wheat-pea mixtures. Ann Bot 114:725-737.

Barth R, IJsselmuiden J, Hemming J, Van Henten EJ (2018) Data synthesis methods for semantic segmentation in agriculture: A *Capsicum annuum* dataset. Comput Eletron Agr 144:284-296.

Burgess AJ, Retkute R, Herman T, Murchie EH (2017) Exploring relationships between canopy architecture, light distribution, and photosynthesis in

contrasting rice genotypes using 3D canopy reconstruction. Front Plant Sci 8:734.

Burgess AJ, Retkute R, Pound MP, Foulkes J, Preston SP, Jensen OE, Murchie EH (2015) High-resolution three-dimensional structural data quantify the impact of photoinhibition on long-term carbon gain in wheat canopies in the field. Plant Physiol 169:1192-1204.

Chaudhury A, Barron JL (2018) Machine vision system for 3D plant phenotyping. IEEE ACM T Comput Bi.

Chelle M, Andrieu B (1998) The nested radiosity model for the distribution of light within plant canopies. Ecol Modell 111:75-91.

Cieslak M, Lemieux C, Hanan J, Prusinkiewicz P (2008) Quasi-Monte Carlo simulation of the light environment of plants. Funct Plant Biol 35:837-849.

Coussement J, Steppe K, Lootens P, Roldán-Ruiz I, De Swaef T (2018) A flexible geometric model for leaf shape descriptions with high accuracy. Silva Fenn 52:7740.

De Reffye P, Heuvelink E, Guo Y, Hu BG, Zhang BG (2009) Coupling process-

based models and plant architectural models: a key issue for simulating crop production. In Crop Modeling and Decision Support, p. 130-147. Springer, Berlin, Germany.

De Visser PHB, van der Heijden G, Buck-Sorlin G (2014) Optimizing illumination in the greenhouse using a 3D model of tomato and a ray tracer. Front Plant Sci 5:48.

Falster DS, Westoby M (2003) Leaf size and angle vary widely across species: What consequences for light interception? New Phytol 158:509-525.

Farquhar GD, Roderick ML (2003) Pinatubo, diffuse light, and the carbon cycle. Science 299:1997-1998.

Godin C, Sinoquet H (2005) Functional-structural plant modelling. New Phytol 166:705-708.

Hosoi F, Omasa K (2015) Estimating leaf inclination angle distribution of broad-leaved trees in each part of the canopies by a high-resolution portable scanning Lidar. J Agric Meteorol 71:136-141.

Jordan DN, Smith WK (1993) Simulated influence of leaf geometry on sunlight interception and photosynthesis in conifer needles. Tree Physiol 13:29-39.

Jovicich E, Cantliffe DJ, Stoffella PJ (2004) Fruit yield and quality of greenhouse-grown bell pepper as influenced by density, container, and trellis system. HortTechnology 14:507–513.

Kim, JH, Lee JW, Ahn TI, Shin JH, Park KS, Son JE (2016) Sweet pepper (*Capsicum annuum L.*) canopy photosynthesis modeling using 3D plant architecture and light ray-tracing. Front Plant Sci 7:1321.

Li T, Heuvelink E, Dueck TA, Janse J, Gort G, Marcelis LFM (2014) Enhancement of crop photosynthesis by diffuse light: Quantifying the contributing factors. Ann Bot 114:145-156.

Li T, Kromdijk J, Heuvelink E, Van Noort FR, Kaiser E, Marcelis LF (2016) Effects of diffuse light on radiation use efficiency of two *Anthurium* cultivars depend on the response of stomatal conductance to dynamic light intensity. Front Plant Sci 7:56.

Lindenmayer A (1968) Mathematical models for cellular interactions in development. I. Filaments with one-sided inputs. J Theor Biol 18:280-299.

Lou L, Liu Y, Han J, Doonan JH (2014) Accurate multi-view stereo 3D reconstruction for cost-effective plant phenotyping. Inti Image Anal

Recog 8815:349-356.

Mercado LM, Bellouin N, Sitch S, Boucher O, Huntingford C, Wild M, Cox PM (2009) Impact of changes in diffuse radiation on the global land carbon sink. Nature 458:1014.

Moriondo M, Leolini L, Staglianò N, Argenti G, Trombi G, Brilli L, Bindi M (2016) Use of digital images to disclose canopy architecture in olive tree. Sci Hortic 209:1-13.

Niinemets Ü (2007) Photosynthesis and resource distribution through plant canopies. Plant Cell Environ 30: 1052-1071.

Niinemets Ü, Fleck S (2002) Petiole mechanics, leaf inclination, morphology, and investment in support in relation to light availability in the canopy of *Liriodendron tulipifera.* Oecologia 132:21-33.

Paulus S, Schumann H, Kuhlmann H, Léon J (2014) High-precision laser scanning system for capturing 3D plant architecture and analysing growth of cereal plants. Biosyst Eng 121:1-11.

Prusinkiewicz P, Hanan J (1990) Visualization of botanical structures and processes using parametric L-systems, p. 183-201. In: Scientific

visualization and graphics simulation. John Wiley & Sons, New York, NY, USA.

Purcell LC, Ball RA, Reaper JD, Vories ED (2002) Radiation use efficiency and biomass production in soybean at different plant population densities. Crop Sci 42:172-177.

Qian T, Elings A, Dieleman JA, Gort G, Marcelis LFM (2012) Estimation of photosynthesis parameters for a modified Farquhar-von Caemmerer-Berry model using simultaneous estimation method and nonlinear mixed effects model. Environ Exp Bot 82:66-73.

Retkute R, Townsend AJ, Murchie EH, Jensen OE, Preston SP (2018). Three-dimensional plant architecture and sunlit–shaded patterns: A stochastic model of light dynamics in canopies. Ann Bot.

Sarlikioti V, de Visser PH, Buck-Sorlin GH, Marcelis LFM (2011a) How plant architecture affects light absorption and photosynthesis in tomato: Towards an ideotype for plant architecture using a functional-structural plant model. Ann Bot 108:1065-1073.

Sarlikioti, V, De Visser, P. H. B, Marcelis, L. F. M (2011b) Exploring the

spatial distribution of light interception and photosynthesis of canopies by means of a functional-structural plant model. Ann Bot, 107:875-883.

Sinoquet H, Thanisawanyangkura S, Mabrouk H, Kasemsap P (1998) Characterization of the light environment in canopies using 3D digitizing and image processing. Ann Bot 82:203-212.

Townsend AJ, Retkute R, Chinnathambi K, Randall JW, Foulkes J, Carmo-Silva E, Murchie EH (2018) Suboptimal Acclimation of Photosynthesis to Light in Wheat Canopies. Plant Physiol 176:1233-1246.

Ubbens JR, Stavness I (2017) Deep plant phenomics: A deep learning platform for complex plant phenotyping tasks. Front Plant Sci 8:1190.

Van der Heijden, Song Y, Horgan G, Polder G, Dieleman A, Bink M, Glasbey C (2012) SPICY: Towards automated phenotyping of large pepper plants in the greenhouse. Funct Plant Biol 39:870-877.

Vos J, Evers JB, Buck-Sorlin GH, Andrieu B, Chelle M, De Visser PH (2010) Functional-structural plant modelling: A new versatile tool in crop science. J Exp Bot 61:2101-2115.

Wen W, Li B, Li BJ, Guo X (2018) A leaf modeling and multi-scale remeshing

method for visual computation via hierarchical parametric vein and margin representation. Front Plant Sci 9:783.

Yin X, Struik PC (2009) C3 and C4 photosynthesis models: An overview from the perspective of crop modelling. NJAS-Wagen J Life Sc 57:27-38.

Zhang Y, Teng P, Shimizu Y, Hosoi F, Omasa K (2016) Estimating 3D leaf and stem shape of nursery paprika plants by a novel multi-camera photography system. Sensors 16:874.

Zhang YH, Liang T, Liu XJ, Liu LL, Cao WX, Yan Z (2017) Modeling curve dynamics and spatial geometry characteristics of rice leaves. J Integr Agric 16: 2177-2190.

Zotz G, Reichling P, Valladares F (2002) A simulation study on the importance of size-related changes in leaf morphology and physiology for carbon gain in an epiphytic bromeliad. Ann Bot 90:437-443.

ABSTRACT IN KOREAN

식물체의 구조는 식물의 광환경 및 광합성에 영향을 주는 중요한 요인 중 하나이다. 기존의 구조-기능 식물 모델은 식물체의 수광 분석에 많이 사용되었지만, 구조적 정확성이 떨어지기 때문에 수광 및 이후의 광합성에 영향을 줄 수 있다. 본 연구의 목적은 3차원 스캐너를 통해 구축한 모델과, 기존 방식의 모델에서 수광과 광합성이 어떻게 다른지 확인하는 것이다. 단일 엽 수준에서는 스캔 데이터에서 직접 구축한 모델과, 기존 방식의 낮은 곡률의 잎을, 식물 개체 수준에서는 스캔 데이터를 통해 구축한 모델과, 스캔 모델에서 측정한 식물 구조 변수를 상업용 소프트웨어에 대입하여 만든 정적 모델을 비교하였다. 두 식물 모델에 같은 조건으로 잎과 개체 단위에서 광추적 시뮬레이션을 통해 수광 분석을 한 뒤, 얻어진 수광 값을 FvCB 모델에 적용하여 광합성을 계산하였다. 그 결과, 잎과 개체 수준에서 관행 모델에서 엽맥과 같은 세밀한 구조의 생략에 의해 수광량이 스캔 모델에 비해 과대 평가되었으며, 구조 표현에 따른 광도 분포의 차이에 의해서 수광 이후의 광합성 또한 더 높게 평가되는 것을 확인할 수 있었다. 특히 식물 개체 수준에서의 수광량과 광합성 속도가 각각 30과, 59% 높게 평가되는 것을 확인하였다. 따라서 3차원 스캔-재구축 방식을

이용한 식물 모델을 이용하면 보다 정밀하게 식물 수관의 수광 및 광합성을 할 수 있을 것이다.

추가 주요어: 광추적, 광합성, 식물 구조, 3차원 스캐닝, 3차원 파라메트릭 모델, 파프리카

학 번: 2017-23794

SUPPLEMENTARY INFORMATION

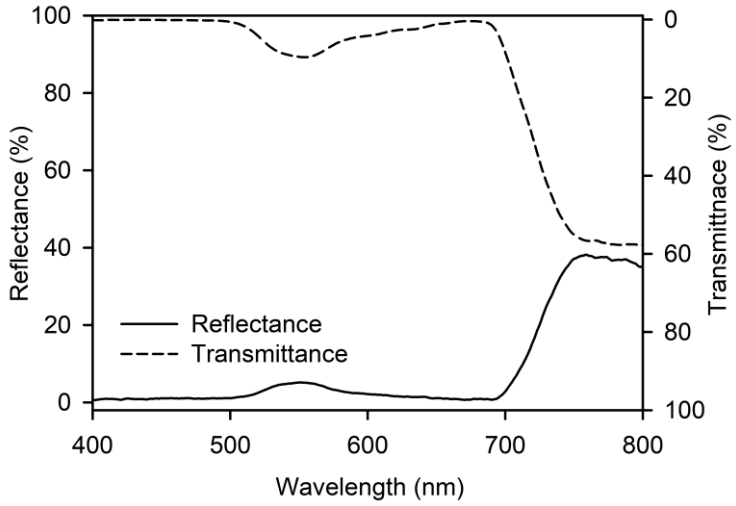

Fig. S1. Measured leaf transmittance and reflectance of sweet pepper plants at 400-700 nm.

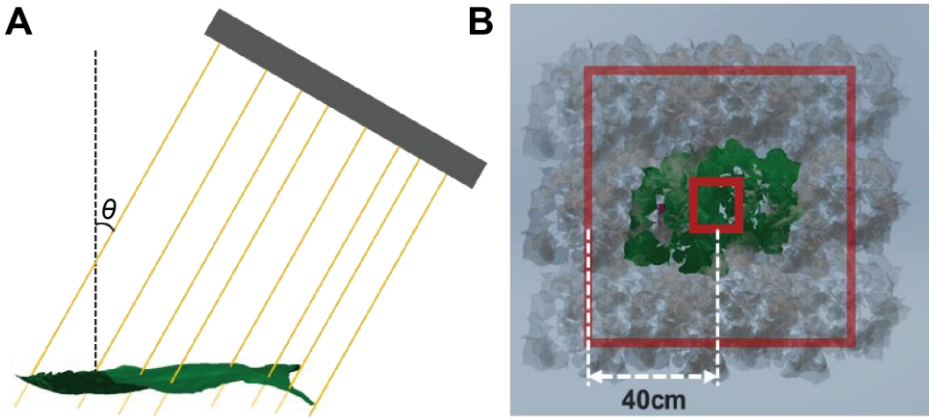

Fig. S2. Ray-tracing simulation conditions at leaf and whole-plant levels. (A) Simulation conditions for a leaf. Incoming radiation angle (θ) was the angle between ray direction and zenith direction, and a direct light source was used. (B) Simulation conditions for a whole-plant. Plants had a 3 x 3 isotropic arrangement and were separated by a distance of 40 cm.

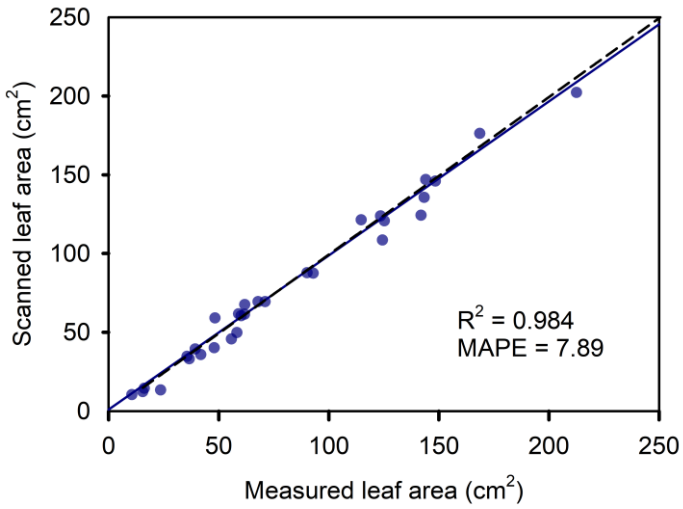

Fig. S3. Leaf areas measured by 3D scanning or mechanical measurement. Dashed and solid lines represent the 1:1 line and regression line, respectively.

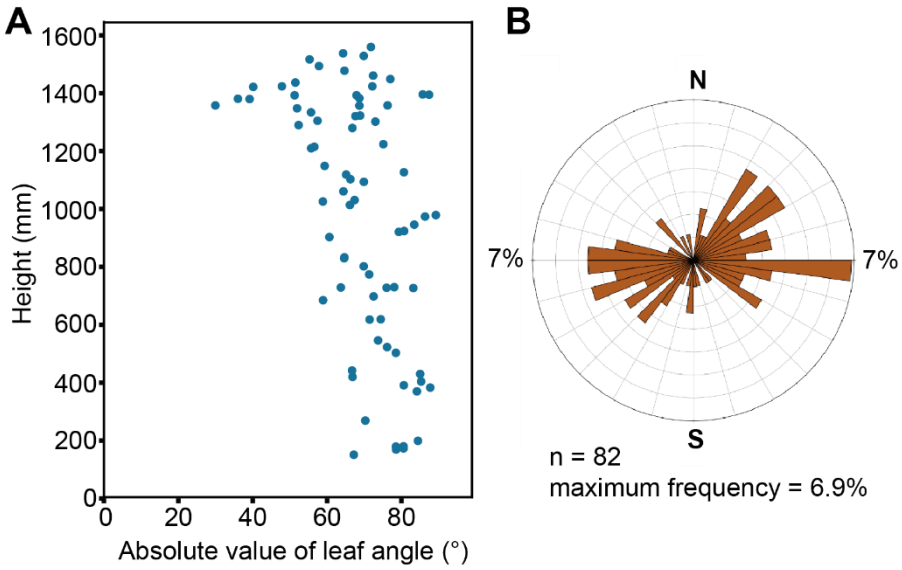

Fig. S4. Architectural parameters of a plant used to create a 3D plant model. (A) Leaf angle distribution according to height and (B) positional distribution. East and west were the trained directions of the two main stems.

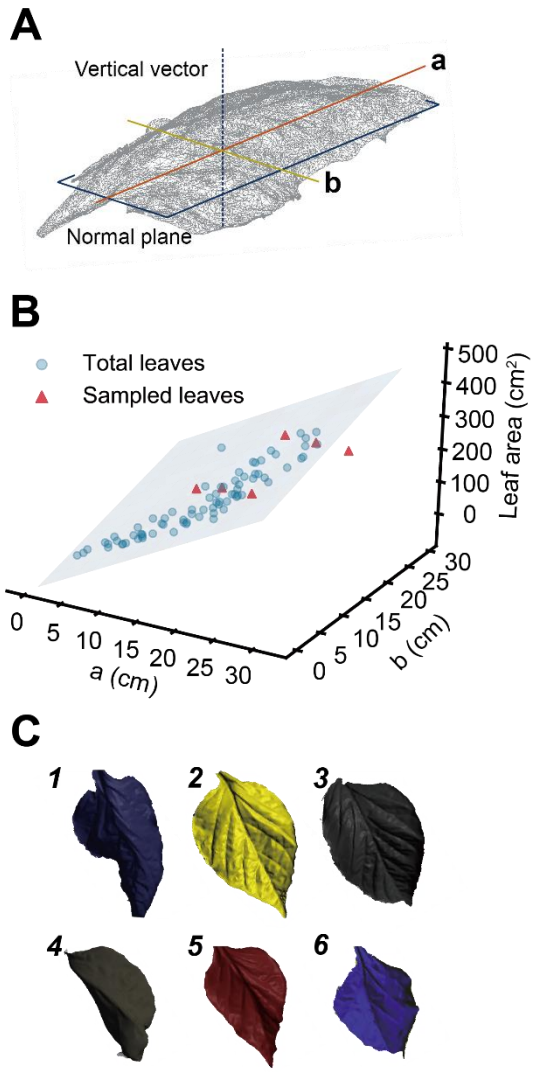

Fig. S5. Physical characteristics of sampled leaves. (A) Description of straight distances of leaf length *a* and width *b*, and (B) relationships between *a*, *b* value and leaf area of sampled leaves. (C) Scanned meshes of six sampled leaves.

Table S1. Parameters of the FvCB model used to calculate photosynthetic rates at the top, middle, and bottom layers of the plant.

Parameter	Top	Middle	Bottom
V_{cmax}	81.9	37.0	14.6
J_{max}	162.4	38.4	12.3